

UC Riverside

2017 Publications

Title

Reduction of air pollution levels downwind of a road with an upwind noise barrier

Permalink

<https://escholarship.org/uc/item/2950k8f2>

Journal

Atmospheric Environment, 155

ISSN

13522310

Authors

Enayati Ahangar, Faraz
Heist, David
Perry, Steven
[et al.](#)

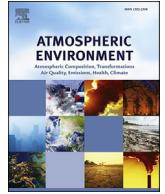
Publication Date

2017-04-01

DOI

10.1016/j.atmosenv.2017.02.001

Peer reviewed



Reduction of air pollution levels downwind of a road with an upwind noise barrier



Faraz Enayati Ahangar^a, David Heist^b, Steven Perry^b, Akula Venkatram^{a,*}

^a University of California, Riverside, CA 92521, USA

^b US Environmental Protection Agency, Office of Research and Development, Research Triangle Park, NC 27711, USA

HIGHLIGHTS

- Upwind barrier reduces downwind near-road pollutant concentrations.
- Dispersion model accounts for upwind barrier.
- Recirculation behind barrier pushes emissions upwind.
- Can be as effective as downwind barrier.
- Increases impact of downwind barrier.

ARTICLE INFO

Article history:

Received 13 July 2016

Received in revised form

1 February 2017

Accepted 2 February 2017

Available online 3 February 2017

Keywords:

Dispersion modeling

Noise barrier

Near-road concentration

Air pollution

Recirculation zone

ABSTRACT

We propose a dispersion model to estimate the impact of a solid noise barrier upwind of a highway on air pollution concentrations downwind of the road. The model, based on data from wind tunnel experiments conducted by Heist et al. (2009), assumes that the upwind barrier has two main effects: 1) it creates a recirculation zone behind the barrier that sweeps the emissions from the highway back towards the wall, and 2) it enhances vertical dispersion and initial mixing. By combining the upwind barrier model with the mixed wake model for a downwind barrier described in Schulte et al. (2014), we are able to model dispersion of emissions from a highway with noise barriers on both sides. The model provides a good description of measurements made in the wind tunnel. The presence of an upwind barrier causes reductions in concentrations relative to those measured downwind of a road with no barriers. The reduction can be as large as that caused by a downwind barrier if the recirculation zone covers the width of the highway. Barriers on both sides of the highway result in larger reductions downwind of the barriers than those caused by a single barrier either upwind or downwind. As expected, barrier effects are small beyond 10 barrier heights downwind of the highway. We also propose a tentative model to estimate on-road concentrations within the recirculation zone induced by the upwind barrier.

© 2017 Elsevier Ltd. All rights reserved.

1. Introduction

Several field and laboratory studies indicate that noise barriers next to roads reduce near-road concentration of pollutants emitted by vehicles. Because these barriers are designed to reduce the impact of road noise on adjacent residential areas, they can be located on both sides of the road or only on one side. In this paper, we refer to a barrier as “upwind” if the road is downwind of the barrier when the wind blows across the road. It is referred to as

“downwind” otherwise.

A field study near interstate I-440, Raleigh, North Carolina, showed that the presence of a downwind noise barrier can reduce concentrations of CO and PM number by up to 50% downwind of the barrier (Baldauf et al., 2008). A study at the Idaho National Laboratory that released a tracer gas, sulfur hexafluoride, from a line source upwind of a barrier (Finn et al., 2010) showed similar reductions in tracer concentrations downwind of the barrier under all meteorological conditions. A wind tunnel study examined the effect of different configurations including downwind solid barriers, upwind barriers, depressed highways, and elevated highways on near-road pollutant concentrations and found that all of these configurations result in reductions of near-road concentrations

* Corresponding author.

E-mail address: venkatram@sbcglobal.net (A. Venkatram).

compared to those for a flat roadway with no barriers except for an elevated highway where the source is elevated on a sloped embankment. (Heist et al., 2009).

These results from field and laboratory studies are supported by simulations using a Computational fluid dynamics (CFD) model, which shows that downwind roadside barriers result in reduced concentrations behind the barrier (Hagler et al., 2011). Steffens et al. (2014) developed a CFD model based on Large-Eddy Simulation and found that roadside barriers, elevated highways, depressed highways, and combinations of these configurations reduced near-road concentrations. Schulte et al. (2014) developed a semi-empirical model to estimate concentrations in the presence of a downwind barrier and evaluated it with data from the Idaho Falls experiment (Finn et al., 2010) and wind tunnel data (Heist et al., 2009). However, none of these modeling studies examined the impact of single barriers upwind of the road, or barriers on both sides of the road.

In this paper, we propose a semi-empirical model to estimate the effects of upwind barriers on near-road pollutant concentrations. The impact of barriers on both sides of the highway is modeled using the upwind barrier model in combination with the mixed-wake model (Schulte et al., 2014) formulated to estimate the effect of a downwind barrier. The models are evaluated using the data collected by Heist et al. (2009) in a wind tunnel study. These semi-empirical models are useful because they capture the fundamental physics governing the effects of solid barriers on the dispersion of pollutants, and yet are anchored to observations through frameworks that facilitate application to real-world situations.

2. Wind tunnel measurements

Heist et al. (2009) conducted a wind tunnel study to examine the near-road impact of emissions from a simulated six-lane divided highway modeled at 1:150 scale. They considered twelve roadway configurations (Table 1), including seven with solid noise barriers at different heights and locations. Five of the seven barrier cases are used in this examination of upwind barrier effects. The study was conducted in the meteorological wind tunnel at U.S. EPA's Fluid Modeling Facility (Snyder, 1979). The wind tunnel test section measures 370 cm wide by 210 cm high and 1830 cm long (Fig. 1). The boundary layer wind profile was generated with a combination of Irwin spires (Irwin, 1981) at the inlet and roughness blocks arrayed on the floor to condition the flow to simulate a typical atmospheric boundary layer profile. The typical barrier height, H , at full scale was 6 m. Four cases, G, L, J, and K, involved only upwind barriers. Case I examined two 6 m barriers, one on each side of the highway. All of the cases used a neutral boundary

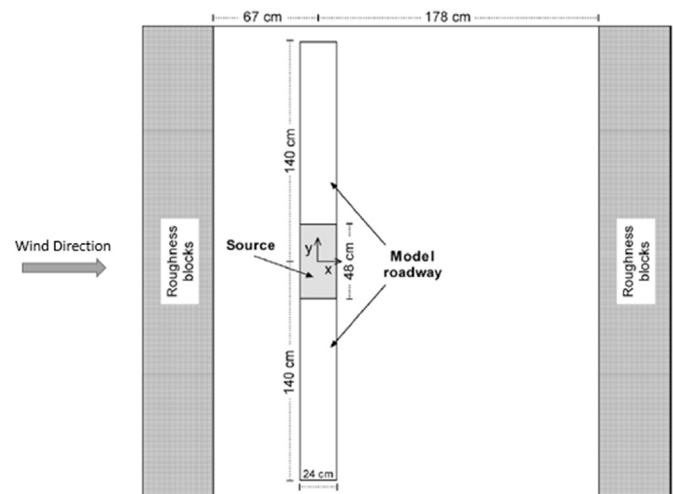


Fig. 1. Layout of the wind tunnel study (Heist et al., 2007).

layer with a surface roughness, $z_0 = 0.52$ cm (0.78 m full scale), and a friction velocity, $u_* = 0.3 \frac{m}{s}$ and a displacement height $d = 5.4$ cm (8.1 m full scale). A near-neutrally-buoyant tracer gas (ethane) was released from six lines along the roadway, and downwind concentration samples were collected through tubes mounted on the wind tunnel carriage system. Tracer concentrations were measured using hydrocarbon analyzers (flame ionization detectors) to form concentration profiles. Velocity measurements were obtained with a two-component laser Doppler velocimetry (LDV) system.

2.1. Upwind barrier cases

Fig. 2 shows the configuration of each upwind barrier case modeled in Heist et al. (2009). Dimensions are in full scale.

Fig. 3, which depicts the velocity profiles for the two single barrier cases, G and H, shows that the length of the recirculation zone behind the barrier is about 6 barrier heights. Note that H corresponds to a single barrier located downwind of the road. As expected, the velocity field around a single barrier does not depend on its location.

However, as Fig. 4 shows, the recirculation zone extends 4 barrier heights behind the upwind barrier when there are two barriers on both sides of the highway. This observation is used in formulating the model for dispersion in the presence of two barriers. This is consistent with studies (Becker et al., 2002; Schulman et al., 2000) that show that the extent of the recirculation zone depends on the height of the barrier, the width of the road, the aspect ratio, and the type of boundary layer.

3. Barrier models

3.1. Upwind barrier model

We see from the wind tunnel measurements, shown in Figs. 3 and 4, that the flow in the recirculation zone is directed towards the upwind barrier close to the highway surface. This flow transports the pollutants emitted within the recirculation zone towards the barrier in the upwind direction. This feature is also observed in street canyons on the leeward side of the street and is incorporated in the Operational Street Pollution Model (OSPM, Berkowicz, 2000). In the proposed model, we assume that the emissions on the highway that are covered by the recirculation zone originate from a

Table 1
Case descriptions in the wind tunnel study.

Case	Description
A	Flat terrain
B	Elevated source, 1H, 30° walls
C	Depressed source, 1H, 90° walls
D	Depressed source, 1.5H, 90° walls
E	Depressed source, 1H, 30° walls
F	Depressed source, 1H, 30° walls with noise barriers, 1H tall at upwind and downwind edges.
G	Noise barrier, 1H tall, at upwind edge of the road
H	Noise barrier, 1H tall, at downwind edge of the road
I	Noise barriers, 1H tall, at upwind and downwind edges of the road
J	Noise barrier, 1.5H tall, at upwind edge of the road
K	Noise barrier, 1H tall, 1H upwind of upwind edge of the road
L	Noise barrier, 1H tall, 2H upwind of upwind edge of the road

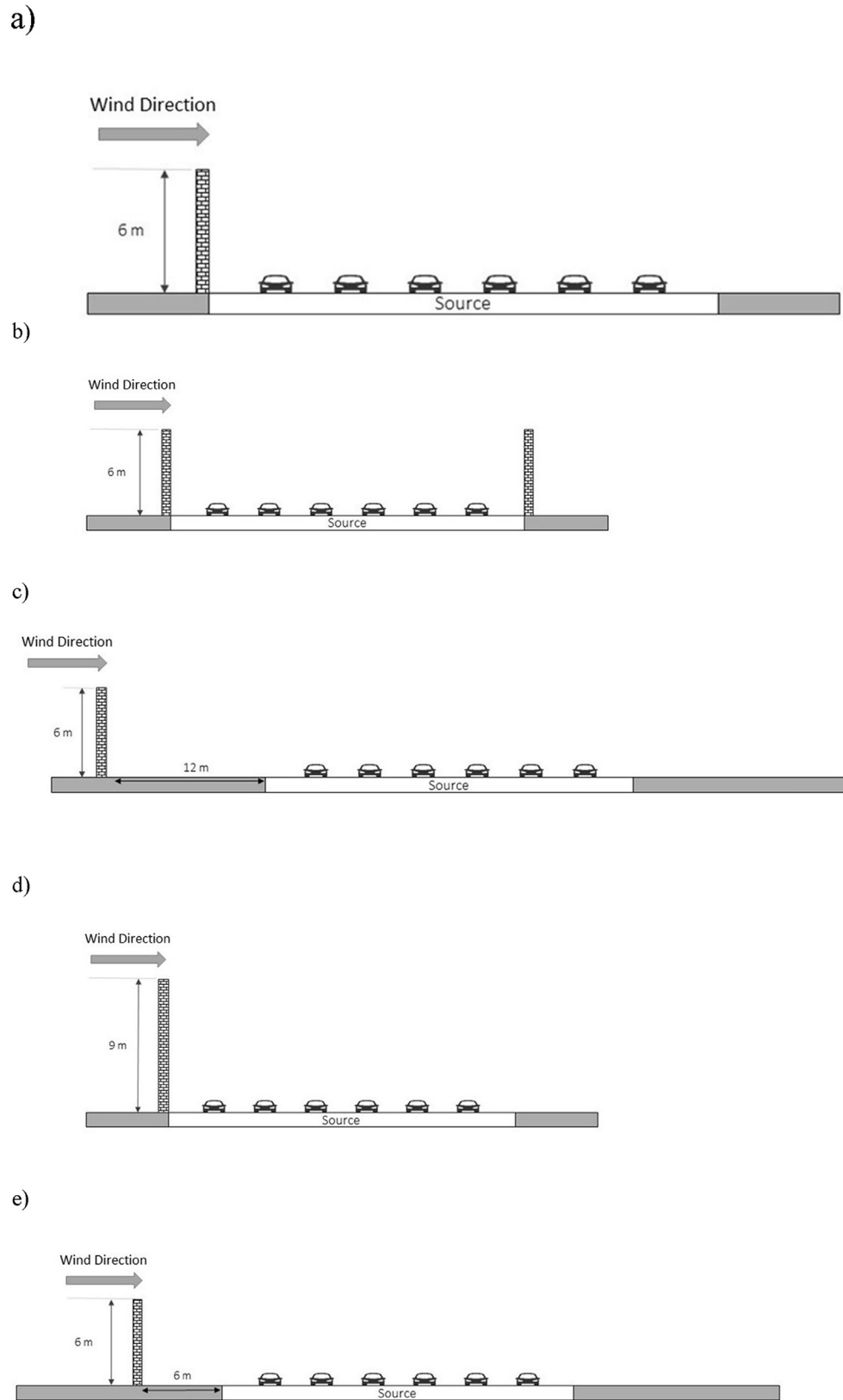


Fig. 2. Different upwind barrier configurations, a) case G, b) case I, c) case L, d) case J, and e) case K.

line source located on the upwind barrier at half the height of the barrier. The sources outside the recirculation zone contribute directly to the downwind receptors (See Fig. 5).

We model the concentration associated with the line source using the approximation proposed by Venkatram and Horst (2006):

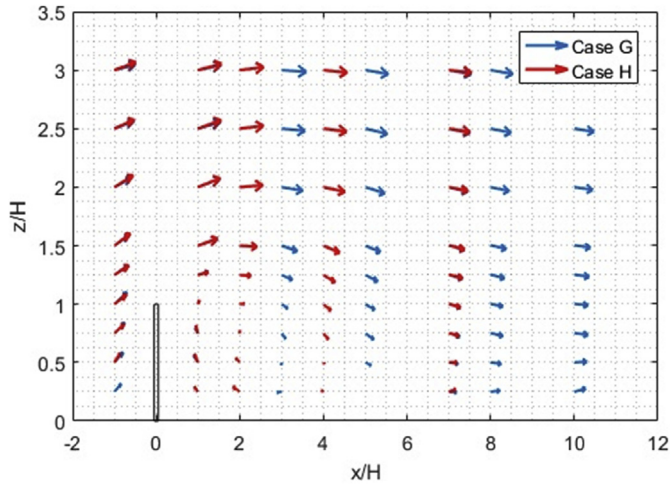


Fig. 3. Wind velocity vectors in the presence of a solid barrier for case G and case H from the wind tunnel data. Dimensions are shown in barrier height (H) and the upwind barrier is located at $\frac{x}{H} = 0$.

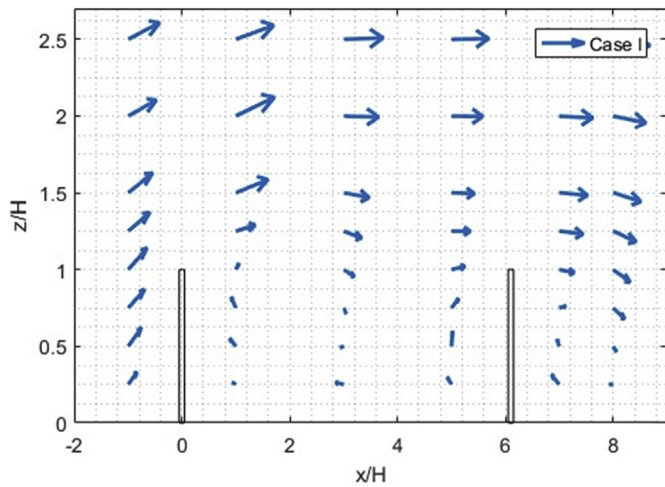


Fig. 4. Wind velocity vectors in the presence of two solid barriers for case I from the wind tunnel data. Dimensions are multiples of barrier height (H) and the upwind barrier is located at $\frac{x}{H} = 0$.

$$C(x,z) = \frac{q}{U(\bar{z})\cos\theta\sqrt{2\pi}\sigma_z(x/\cos\theta)} \left[\exp\left(-\frac{(z_s-z)^2}{2\sigma_z(x)^2}\right) + \exp\left(-\frac{(z_s+z)^2}{2\sigma_z(x)^2}\right) \right] \quad (1)$$

Where q is the emission rate per unit of length and θ is the angle of the wind direction perpendicular to the line source. In this equation, x is the downwind distance from the line source, z is the receptor height, z_s is the source height, σ_z is vertical plume spread, h is the source height, and $U(\bar{z})$ is the wind speed evaluated at the effective plume centerline height, \bar{z} , defined by:

$$\bar{z} = \frac{\int_0^\infty zC^y(x,z)dz}{\int_0^\infty C^y(x,z)dz} \quad (2)$$

The height of this line source is taken to be half of the barrier height. The sources outside the recirculation are treated as line sources at ground-level at various distances from the receptor (Fig. 5). The effect of the downwind barrier on these sources is described in Schulte et al. (2014). This model, referred to as the mixed-wake model, assumes that the concentration is uniform below barrier height, which results in the following expression for the near surface concentration, C_s :

$$C_s = \frac{q}{U(\bar{z})\cos\theta\sqrt{\frac{\pi}{2}}\sigma_z(x/\cos\theta) + U\left(\frac{H}{2}\right)H\cos\theta} \quad (3)$$

Where x is the downwind distance from the line source, H is the barrier height, and $U\left(\frac{H}{2}\right)$ is the wind speed at half of the barrier height. The model was evaluated using wind tunnel data (Heist et al., 2009) and tracer study data (Finn et al., 2010), and showed good performance with measurements.

Plume spreads are calculated using the following equations:

$$\sigma_z = \sqrt{\sigma_{z_p}^2 + \sigma_{z_0}^2} \quad (4)$$

Where σ_{z_0} is the initial vertical plume spread and σ_{z_p} is calculated using the following equations (Venkatram et al., 2013):

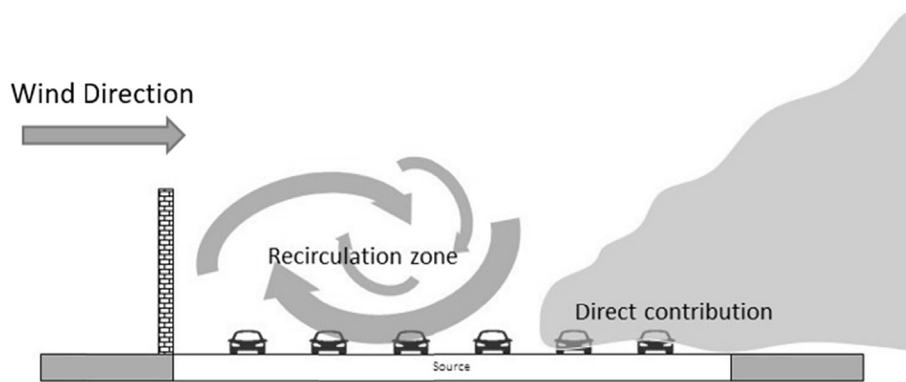


Fig. 5. Recirculation zone and direct contribution in the upwind barrier model.

$$\sigma_{zp} = \alpha * 0.57 \frac{u_*}{U(\bar{z})} x \frac{1}{1 + 3 \frac{u_*}{U(\bar{z})} \left(\frac{x}{L}\right)^{2/3}}, L > 0 \tag{5a}$$

$$\sigma_{zp} = \alpha * 0.57 \frac{u_*}{U(\bar{z})} x \left(1 + 2 \frac{u_*}{U(\bar{z})} \frac{x}{|L|}\right), L < 0 \tag{5b}$$

here u_* is the surface friction velocity, L is the Monin-Obukhov length, and α accounts for increased rate of plume spread caused by the barrier. It has the following form (Schulte et al., 2014):

$$\alpha = 1 + \frac{b(U(H)/u_*)^2}{1 + \left(\frac{x}{20H}\right)^{1/2}} \tag{6}$$

The empirical constant b is set to 0.035 to fit with measurements. We assume that initial vertical spread of plume, σ_{z0} , induced by the barrier is related to the barrier height through $\sigma_{z0} = \beta H$ (Venkatram, 2013). $\beta = 0.25$ was selected to fit the measurements. The effects of two barriers, one upwind of the source and one downwind of the source, on dispersion is modeled by assuming that the effects from upwind and downwind models are independent and can be thus added linearly.

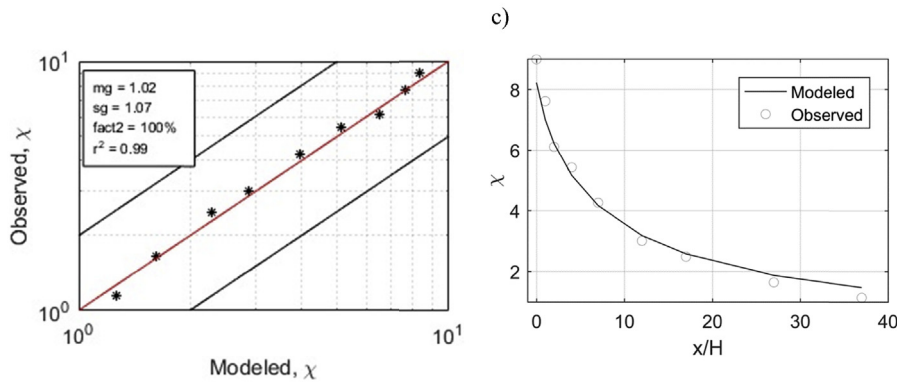
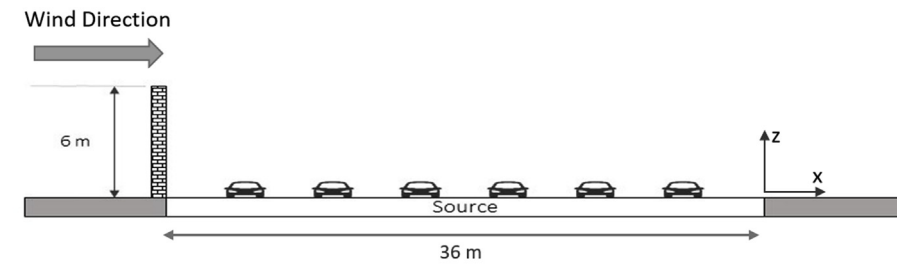
Part b of Figs. 6–9 compare ground-level concentrations measured in a wind tunnel study with corresponding model estimates. Model performance is measured using the following statistics of the ratios of the observed to measured concentrations: the geometric mean (m_g), the standard deviation (s_g), the fraction between 0.5 and 2 (fac2) (Venkatram, 2008). We also calculate the correlation coefficient (r^2) between model estimates and

corresponding measurements of ground-level concentrations. Observed concentrations are normalized to yield non-dimensional concentrations $\chi = \frac{CU_r}{L_x L_y}$, where C is the concentration with background subtracted, U_r is reference wind speed, Q is volumetric effluent rate, L_x is the along wind dimension of the roadway segment, and L_y is lateral length of the source segment.

We see that the simple model provides an excellent description of both the magnitudes as well as the spatial distributions of the measured concentrations.

Part c of Figs. 6–9 compares concentrations measured at different downwind distances behind the barrier with corresponding model estimates. Since the pollutants coming from the recirculation zone are modeled as a single line source at the barrier location, the concentrations at the receptors within the recirculation zone are computed using a different model discussed later. Distances are measured from the edge of the highway for all the cases except case J which is from the end of recirculation zone at 9 barrier heights downwind of the upwind barrier. In case G, the model underestimates the concentration by 7 percent at the first receptor but shows better performance at further downwind distances. For case L, the model also underestimates concentrations at the first receptor by about 8 percent and performs better for further downwind distances. In case J, the model underestimates concentration at the first receptor by 9 percent and shows good agreement at rest of downwind distances. On the other hand, for case K, the model overestimates concentrations at all of the downwind distances. The difference between the model estimate and measured value is 18 percent at the first receptor and gradually becomes smaller at further downwind distances.

a) Case G: Noise barrier, 1 H tall at upwind edge of the road.



b)

Fig. 6. a) Barrier configuration, b) comparison of model estimates with observed concentrations, c) performance of model in describing spatial gradients for case G. Co-ordinate system used in modeling is shown.

a) Case L: Noise barrier, 1H tall at 2H upwind of upwind edge of the road.

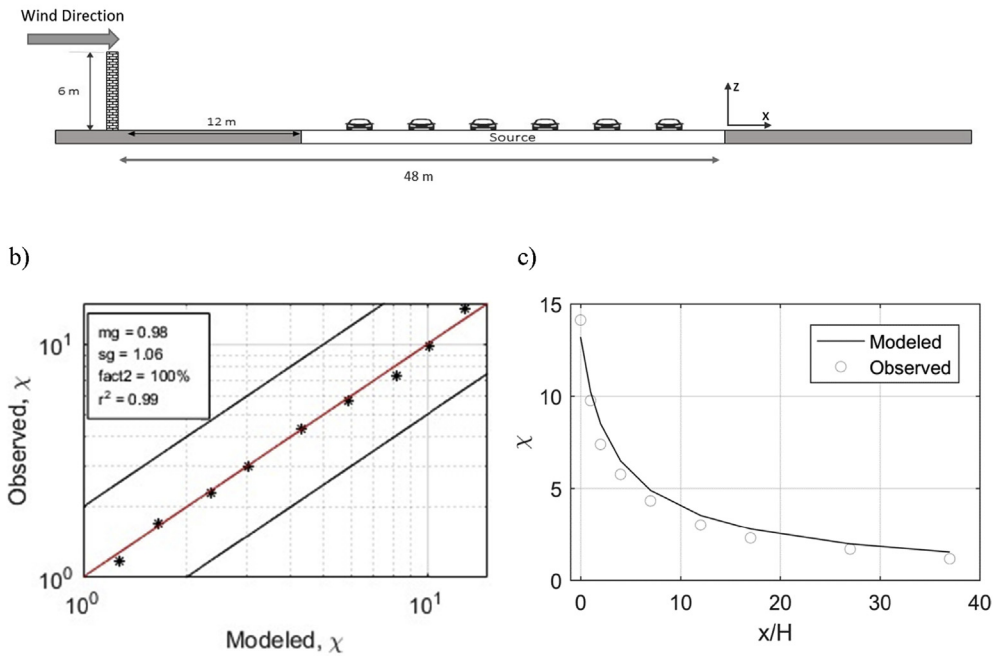


Fig. 7. a) Barrier configuration, b) comparison of model estimates with observed concentrations, c) performance of the model in describing spatial gradients for case L.

a) Case J: Noise barrier, 1.5H tall at upwind edge of the road.

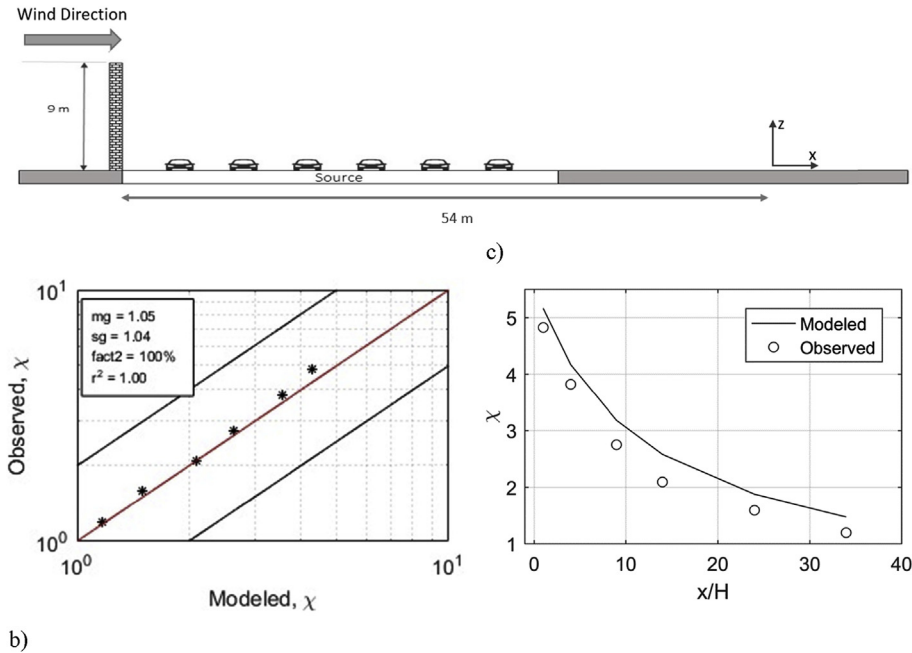


Fig. 8. a) Barrier configuration, b) comparison of model estimates with observed concentrations, c) performance of the model in describing spatial gradients for case J.

3.2. Barriers on both sides of the highway

Case I in the wind tunnel measurements has barriers at both sides of the highway. Wind profiles are shown in Fig. 4. The recirculation zone behind the upwind barrier extends for about 4 barrier heights, which is shorter than the previous case when only one

barrier was present. The portion of the highway within this recirculation zone is modeled with the upwind barrier model and the rest of the highway is modeled using the mixed-wake model.

Fig. 10 shows the model performance with two barriers. The model shows good performance in general.

a) Case K: Noise barrier, 1H tall at 1H upwind of upwind edge of the road.

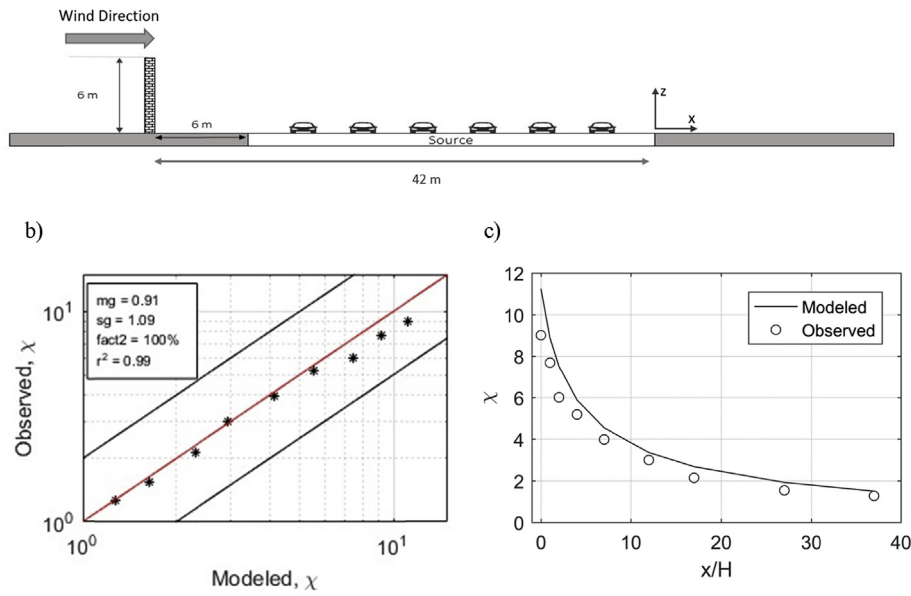


Fig. 9. a) Barrier configuration, b) comparison of model estimates with observed concentrations, c) performance of the model in describing spatial gradients for case K.

a) Case I: Noise barriers, 1H tall at upwind and downwind edges of the road.

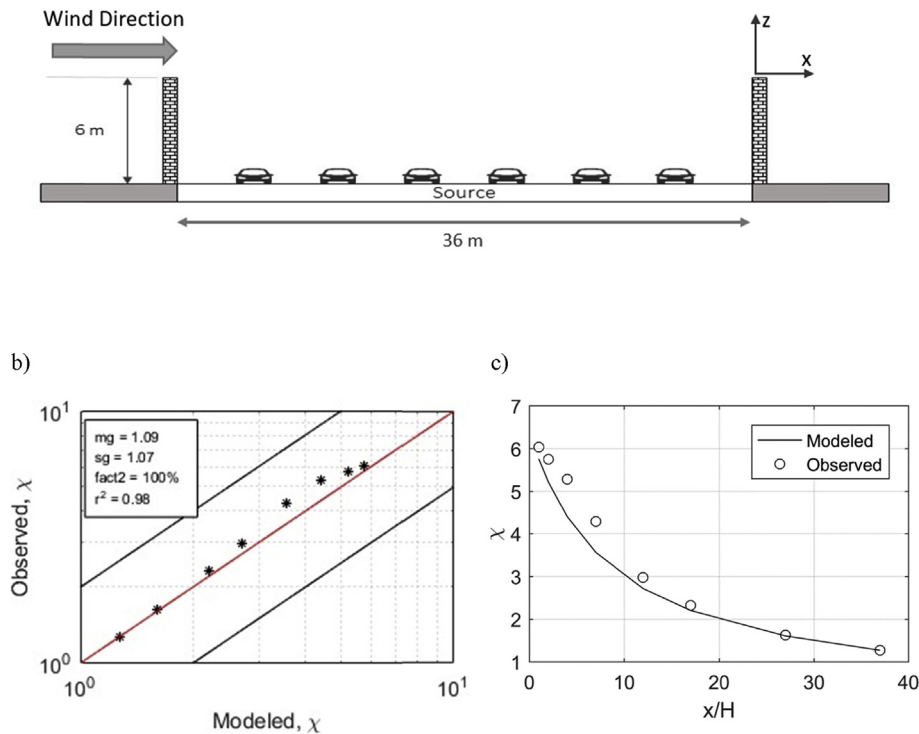


Fig. 10. a) Barrier configuration, b) comparison of model estimates with observed concentrations, c) performance of model in describing spatial gradients for case I.

4. Sensitivity of the model to the height and width of road

4.1. Upwind barrier

Here we estimate the effect of the upwind barrier in reducing

near-road ground-level concentrations relative to the no barrier case. The barrier was located right at the upwind edge of the highway. Three barrier heights were selected, 3 m, 6 m, and 9 m, to represent the range of typical barrier heights.

Fig. 11 shows the spatial concentration variation for the three

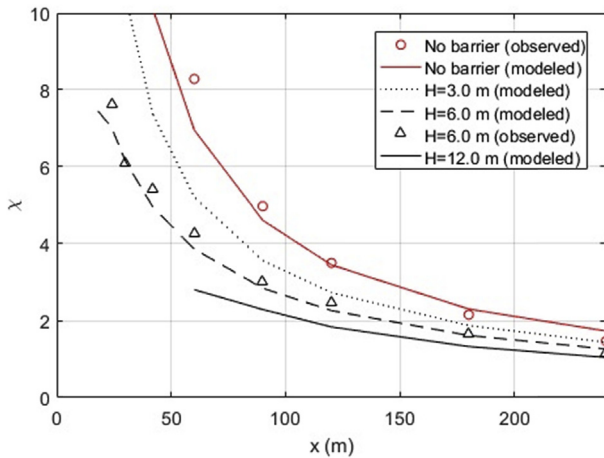


Fig. 11. Model estimates of concentration profiles for upwind barrier with different heights and comparison with measurements. Distances are measured from highway's median.

barrier heights relative to the no barrier case as a function of x/H and x , the downwind distance to compare the effect of different heights, the concentration reduction was considered at two different distances. The first receptor was at $x = 60 \text{ m}$ to exclude the largest recirculation zone extending 54 m for the 9 m barrier. The reduction caused by the 3 m barrier is 26 percent. The 6 m barrier results in a reduction of 44 percent and the 9 m barrier results in a 60 percent reduction. For the 3 m barrier, the recirculation zone covers half of the highway and shifts the emitted pollutant to the barrier location. The emissions outside the recirculation zone have a direct effect on the near road concentrations. In the 6 m and 9 m barrier cases, the recirculation zone covers all of the highway and the difference between concentration gradients are only caused by different initial vertical plume spreads and source heights.

The other receptor is at $x = 240 \text{ m}$ or 40 barrier heights. The reduction for 3 m barrier is only 16 percent at this distance compared with the no barrier case. The reductions for the 6 m and 9 m barriers are 26 percent and 35 percent respectively. As expected, the effect of the barrier on reducing concentrations increases with barrier height, and weakens with downwind distance.

Next, we examined the sensitivity of the model to increasing the highway width. If the recirculation zone covers the whole highway, we see a large reduction comparing to the no barrier case. Increasing the highway width results in reducing the upwind barrier effect because a greater fraction of the emissions lies outside the recirculation zone. Fig. 12 shows the sensitivity of the model to increasing the highway width (W). The concentrations are normalized with the no barrier concentration corresponding to the same highway width.

4.2. Barriers on both sides of the highway

Three different barrier heights are considered to estimate the sensitivity of the model in the presence of two barriers (Fig. 13). The heights are 3 m , 6 m , and 9 m . The reductions caused by barriers are calculated at two different distances. At $x = 60 \text{ m}$, the 3 m barriers cause a 37 percent reduction, the 6 m barriers cause a 49 percent reduction, and the 9 m barriers cause a 66 percent reduction. At $x = 240 \text{ m}$, the 3 m barriers cause only a 17 percent reduction, the 6 m barriers cause a 27 percent reduction, and the 9 m barriers cause a 36% reduction. The effect of two 3 m barriers at both sides of the road is larger than that for one upwind barrier case, while for

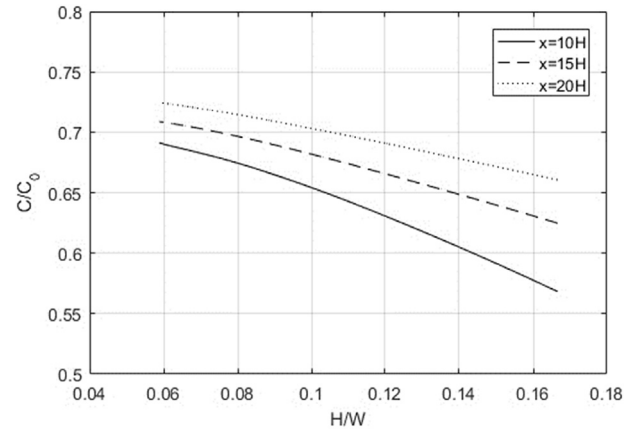


Fig. 12. Sensitivity of the model to increasing highway width. Concentrations are calculated at different distances of $x = 10H$, $x = 15H$, and $x = 20H$ from the center of highway. $H = 6 \text{ m}$.

the 6 m barriers, one or two barriers have almost the same effect.

5. Effects of upwind, downwind, and two barriers on downwind concentrations

Here we compare the effects of different barrier configurations on concentrations downwind of the road. The first configuration is an upwind barrier, which is modeled using the proposed upwind barrier model. The second configuration is a downwind barrier, which is modeled using the mixed-wake model, and the last configuration considers barriers on both sides of the road.

Fig. 14-a compares the measured surface concentration variations behind the barrier for three different configurations with those associated with the no barrier case. The downwind edge of the highway is at $x = 18 \text{ m}$ (3 barrier heights), where the height of barrier for all the cases is 6 m .

The presence of two barriers on both sides of the road causes a 76 percent reduction compared to the no barrier case at one barrier height downwind of the edge of the highway (4 barrier heights or 24 m downwind of the center of the highway). This reduction is 14 percent at 40 barrier heights (240 m). The effects of either upwind or downwind barriers are similar. An upwind or downwind barrier

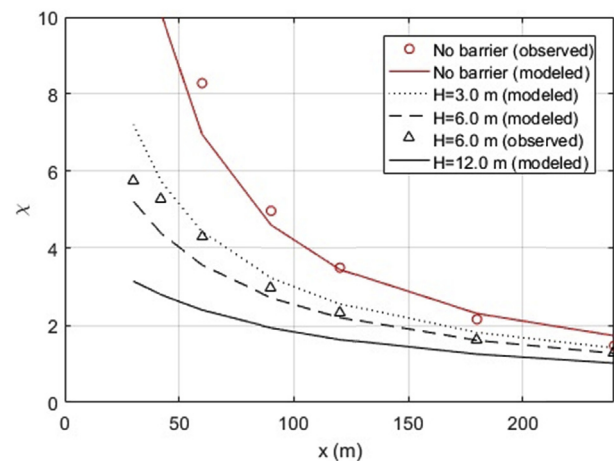


Fig. 13. Model estimates of concentration profiles in presence of barriers on both sides of the highway with different barrier heights and comparison with measurements. Distances are measured from highway's median.

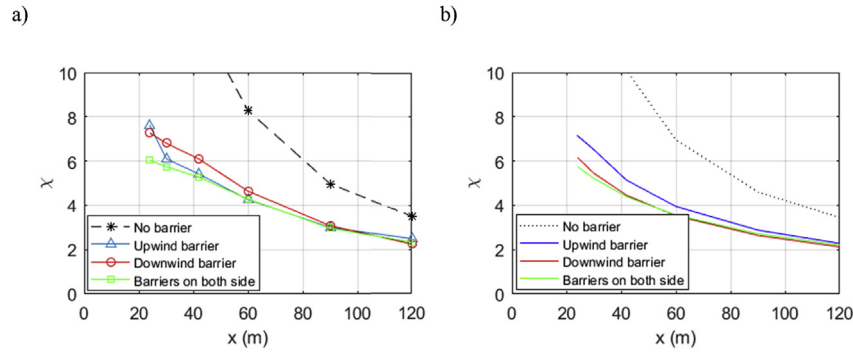


Fig. 14. a) Observed and b) modeled concentration gradients for different barrier configurations. Distances are measured from highway's median.

results in about 70 percent reduction at $x = 24$ and around 20 percent at $x = 240$ m. The concentrations are close to each other at downwind distances beyond 10 barrier heights for all three configurations.

Fig. 14 indicates that the model yields the variation of concentrations similar to that of the measured concentrations. The largest concentration reductions occur for the two barrier case, and the reductions for the one barrier case, either upwind or downwind, are similar. The model predicts a 72 percent reduction for upwind or downwind barriers and a 78 percent reduction in presence of two barriers at both sides of the highway.

The effects of upwind and downwind barriers individually are very close to each other in the wind tunnel. The reason is that in an upwind barrier case, the most effective factor for concentration reduction is the length of recirculation zone. If the recirculation zone covers all of the highway width, which was the case in the wind tunnel study, the barrier has a marked effect on concentration reductions. This is because all of the emissions from the highway are transported towards the upwind barrier. This effect not only shifts the source further from the receptor, but also results in more vertical mixing and pollution dilution.

6. Model for on-road concentrations

The upwind barrier model presented does not estimate concentrations within the recirculation zone where the near surface flow is towards the upwind barrier. Here we present a tentative model to estimate concentrations within this region. Consider a road in which the upwind barrier induces a recirculation zone that extends a distance W_r from the upwind barrier.

We assume that the flow inside this zone carries pollutants towards the barrier in plumes originating from an area source of width W_r , as shown in Fig. 15. Consider a section of the road with

width dp at a distance p from the upwind barrier. The surface concentration associated with this source at a receptor at a distance x from the barrier is (Venkatram et al., 2013):

$$dC = \sqrt{\frac{2}{\pi}} \frac{q}{W} dp \frac{1}{\sigma_z U} \tag{7}$$

where σ_z is evaluated at a distance $(p - x)$ from the source. q is the emission rate per unit length of the road, and W is the total width of the road. The plume spread associated with atmospheric turbulence is given by the neutral expression: $\sqrt{\frac{z}{2}} u(\bar{z}) \sigma_z = \alpha u_* x$ where $\alpha = 0.71$ (Venkatram et al., 2013). We then write

$$\sqrt{\frac{\pi}{2}} \sigma_z U = \alpha u_* (p - x) + h_0 U \tag{8}$$

Here h_0 is the initial plume spread induced by vehicle motion. Inserting Equation (8) into Equation (7) and integrating between the limits x and W_r yields the expression for the surface concentration contributed by the emissions traveling towards the upwind barrier:

$$C_d(x) = \frac{q}{W \alpha u_*} \ln \left(1 + \frac{\alpha u_* (W_r - x)}{h_0 U} \right) \text{ when } x \leq W_r \tag{9}$$

The velocity, U , is evaluated at $h_0 = 1.5$ m. The concentration estimate from Equation (9) is added to the contribution from Equation (1), corresponding to the line source on the upwind barrier.

Model estimates are compared with data from case G which simulated a six-lane highway using line sources consisting of small holes. Blocks with dimensions of $0.6 \times 0.6 \times 1.2$ cm ($0.7 \times 0.9 \times 1.8$ m in real scale) were placed in front of them to enhance near road turbulence. The first receptor in the roadway

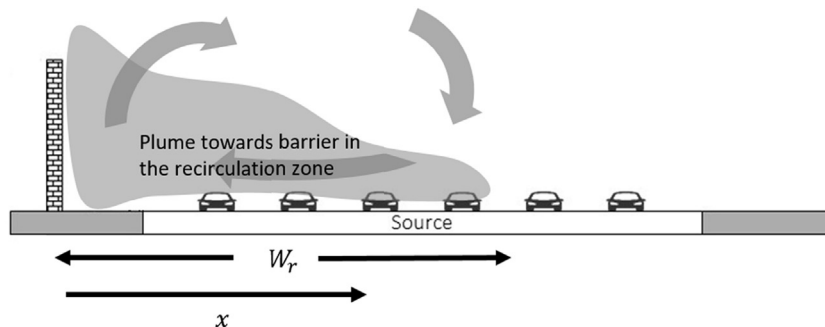


Fig. 15. Schematic illustrating flows assumed in the on-road barrier model.

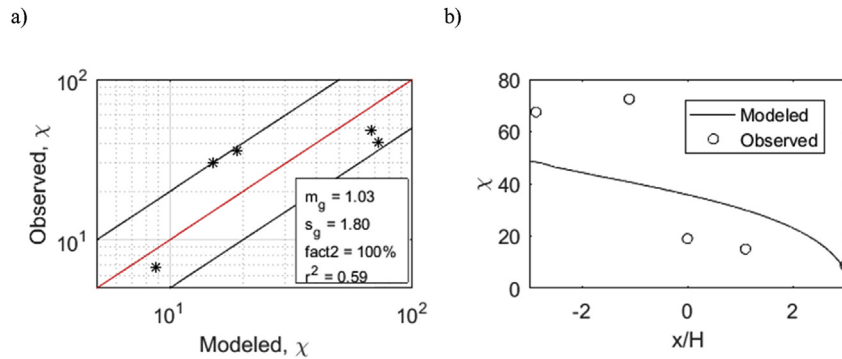


Fig. 16. a) Comparison of modeled with observed values and b) Modeled and observed concentration gradient on the roadway for case G.

was at 0.3 times the barrier height above the surface. We assume that the surface concentration is the same as the concentration measured at 0.3 H in the turbulent recirculation zone.

Fig. 16 compares the modeled surface concentrations and measurements at 0.3 H above the surface for Case G. The correlation between the modeled and observed values is clearly not as good as that for the estimates downwind of the road. However, the concentration estimates are reasonable, within a factor of two of the observations, considering the complexity of the dispersion processes within the cavity of the upwind barrier.

7. Conclusions

A solid barrier at the upwind edge of a highway has significant effects on dispersion of traffic produced emissions. It produces two effects that reinforce each other in reducing downwind concentrations relative to those in the absence of the barrier: it creates a recirculation zone behind the barrier that sweeps the emissions upwind towards the barrier, and at the same time enhances vertical dispersion. We have presented a model to account for these effects.

The model considers the emission sources within the recirculation zone as a single line source at the barrier location and assumes that the initial vertical plume spread is a fraction of the barrier height. By combining this model with the mixed-wake model for the downwind barrier, we are able to simulate the situation with two barriers on both sides of the highway. The models were evaluated with data from the EPA wind tunnel study data and showed generally good agreement with measured values.

The presence of an upwind barrier results in a reduction of downwind concentrations relative to the no barrier case. This reduction increases rapidly with barrier height especially when the height reaches the level at which the recirculation zone covers the entire width of the highway. These results suggest that an upwind barrier that results in a recirculation zone covering the width of a highway can be almost as effective as a downwind barrier. For a single, solid barrier, this width is 6 times the barrier height; for two barriers this width is 4 times the barrier height.

Barriers on both sides of the highway result in a larger concentration reduction than either an upwind or a downwind barrier. Beyond 10 barrier heights downwind of the two barriers, the reductions caused by the three configurations are similar.

Although the model presented here includes the effects of atmospheric stability and near-parallel wind directions, it has only been tested with data from the wind tunnel under neutral conditions when the wind direction is perpendicular to the road. Its

applicability to other conditions requires further evaluation with field data.

Disclaimer

The views expressed here are those of the authors and do not necessarily reflect the views and policies of the U.S. Environmental Protection Agency (EPA). This paper has been subjected to EPA review and approved for publication.

References

- Baldauf, R., Thoma, E., Khlystov, A., Isakov, V., Bowker, G., Long, T., Snow, R., 2008. Impacts of noise barriers on near-road air quality. *Atmos. Environ.* 42, 7502–7507.
- Becker, S., Lienhart, H., Durst, F., 2002. Flow around three-dimensional obstacles in boundary layers. *J. Wind Eng. Ind. Aerodyn.* 90, 265–279.
- Berkowicz, R., 2000. OSPM - a parameterised street pollution model. *Environ. Monit. Assess.* 65, 323–331. <http://dx.doi.org/10.1023/A:1006448321977>.
- Finn, D., Clawson, K.L., Carter, R.G., Rich, J.D., Eckman, R.M., Perry, S.G., Isakov, V., Heist, D.K., 2010. Tracer studies to characterize the effects of roadside noise barriers on near-road pollutant dispersion under varying atmospheric stability conditions. *Atmos. Environ.* 44, 204–214.
- Hagler, G.S.W., Tang, W., Freeman, M.J., Heist, D.K., Perry, S.G., Vette, A.F., 2011. Model evaluation of roadside barrier impact on near-road air pollution. *Atmos. Environ.* 45, 2522–2530. <http://dx.doi.org/10.1016/j.atmosenv.2011.02.030>.
- Heist, D.K., Perry, S.G., Brixey, L.A., Thompson, R.S., Bowker, G.E., 2007. Wind Tunnel Simulation of Flow and Dispersion Near Urban Roadways.
- Heist, D.K., Perry, S.G., Brixey, L.A., 2009. A wind tunnel study of the effect of roadway configurations on the dispersion of traffic-related pollution. *Atmos. Environ.* 43, 5101–5111.
- Irwin, H., 1981. The design of spires for wind simulation. *J. Wind Eng. Ind. Aerodyn.* 7, 361–366.
- Schulman, L.L., Strimaitis, D.G., Scire, J.S., 2000. Development and evaluation of the PRIME plume rise and building downwash model. *J. Air Waste Manage. Assoc.* 50, 378–390.
- Schulte, N., Snyder, M., Isakov, V., Heist, D., Venkatram, A., 2014. Effects of solid barriers on dispersion of roadway emissions. *Atmos. Environ.* 97, 286–295. <http://dx.doi.org/10.1016/j.atmosenv.2014.08.026>.
- Snyder, W.H., 1979. The EPA Meteorological Wind Tunnel: its Design, Construction, and Operating Characteristics, EPA-600/4-79-051. U.S. Environmental Protection Agency Research Triangle Park, NC, p. 78.
- Steffens, J.T., Heist, D.K., Perry, S.G., Isakov, V., Baldauf, R.W., Zhang, K.M., 2014. Effects of roadway configurations on near-road air quality and the implications on roadway designs. *Atmos. Environ.* 94, 74–85. <http://dx.doi.org/10.1016/j.atmosenv.2014.05.015>.
- Venkatram, A., 2008. Computing and displaying model performance statistics. *Atmos. Environ.* 42, 6862–6868.
- Venkatram, A., 2013. Dispersion modeling. *Handb. Environ. Fluid Dyn.* 2, 333–344. <http://dx.doi.org/10.1002/9781118723098>.
- Venkatram, A., Horst, T.W., 2006. Approximating dispersion from a finite line source. *Atmos. Environ.* 40, 2401–2408.
- Venkatram, A., Snyder, M.G., Heist, D.K., Perry, S.G., Petersen, W.B., Isakov, V., 2013. Re-formulation of plume spread for near-surface dispersion. *Atmos. Environ.* 77, 846–855.